Article

Electrokinetic Translocation of a Deformable Nanoparticle through a Nanopore

Teng Zhou,* Jian Ge, Liuyong Shi, Zhenyu Liu, Yongbo Deng, Yinyin Peng, Xiaohan He, Rongnian Tang, and Liping Wen

Cite This: *ACS Appl. Bio Mater.* 2020, 3, 5160−5168

Read Online

ACCESS | Metrics & More | Article Recommendations | Supporting Information

ABSTRACT: The nanopore-based biosensing technology is built up on the fluctuation of the ionic current induced by the electrokinetic translation of a particle penetrating the nanopore. It is expected that the current change of a deformable bioparticle is dissimilar from that of a rigid one. This study theoretically investigated the transient translocation process of a deformable particle through a nanopore for the first time. The mathematical model considers the Poisson equation for the electric potential, the Nernst−Planck equations for the ionic transport, the Navier−Stokes equations for the flow field, and the stress−strain equation for the dynamics of the deformable bioparticle. The arbitrary Lagrangian−Eulerian method is used for the fully coupled particle-fluid dynamic interaction. Results show that the deformation degree of the particle, the velocity deviation, and the current is different from the rigid particle. The deformation degree of the particle will reach the maximum when the particle passes a nanopore. Because of the deformation of particles, the total force applied on deformable particles is larger than that of rigid particles, resulting in larger velocity deviation and current deviation. The influences of the ratio of the nanoparticle radius to the Debye length and surface charge density of the nanopore are also studied. The research results illustrate the translocation mechanism of a deformable nanoparticle in the nanopore, which can provide theoretical guidance for the biosensing technology based on the nanopore.

KEYWORDS: *nanofluidics, arbitrary Lagrangian−Eulerian, nanoparticle translocation, deformation, direct numerical simulation*

1. INTRODUCTION

Nanopores implanted in thin solid membranes are widely used as biosensors for sensing individual bioparticles such as DNA in the past decades.[1−7] In a chamber filled with electrolyte, it is separated by an impermeable membrane in which there is a nanoscale pore. Researchers use electricity, pressure, or other driving methods to make molecules pass through the nanopores, which form a detectable change of current. The mechanism is built up on the temporary deviation of the transmembrane ionic current induced by the electrophoretic motion of a bioparticle translocating through a nanopore.[8−13] Many existing studies have experimentally and theoretically investigated the translocation of a rigid nanoparticle under different conditions. Ai presented a transient continuum-based model to study the electrokinetic particle translocation through a nanopore,[14] and the field-effect regulation of DNA nanoparticle translocation through a nanopore using a gate electrode is investigated later.[15] Others analyzed the electrophoretic motion of a soft spherical nanoparticle in a nanopore and electrokinetic particle translocation through a nanopore containing a floating electrode.[16,17] Furthermore, the local velocity, the effect of pH, and the way to amplify the signal have been studied by many scholars.[18−21] The speed at which the rigid particles passing through the nanopore is essentially

symmetrical and creates current blockade when the particles enter the nanopore.[7,14,16,22−24] Nevertheless, some individual bionanoparticles such as polymers, natural rubber, and DNA molecules are deformable.[10,13,22,24−26] It is expected that the translocation process and current change of a deformable bioparticle should be different from that of a rigid one, the elastic deformation occurs when the particles passing through the nanopore.[17,27] Therefore, it is greatly significant to explore the translocation mechanism of a deformable nanoparticle[28,29] for the further development of the nanopore-based biosensing technology.

In recent years, simulation methods[14−18,30] have been used to illustrate the fundamental translocation process. Limited by the small time scale of the molecular dynamics (MD) method, greater electric field than the actual experimental conditions was typically used in the MD simulations.[14] The simulation conditions in the continuum-based models were closer to the
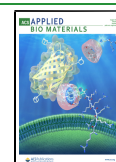
experimental conditions, and their predictions are in good qualitative agreement with both experimental results and the results obtained from MD simulations. Therefore, in the current research, our team adopts a continuum-based model to study the electrokinetic translocation of deformable particles passing through a rigid nanopore. In contrast to the validated model for a rigid particle,[14−18,30] particle deformation described by the stress−strain equation is considered in this research. For the translocation and deformation of the particle, the problem will be numerically solved by the arbitrary Lagrangian−Eulerian (ALE) method.[31−33] The particle's deformation, translating velocity, and the current deviation signal during the dynamic translocation process are investigated as functions of the shear modulus of the deformable nanoparticle, the imposed electric field, the degree of double layer overlapping, and the nanopore's surface electrical property, respectively. The consequences illustrated that the current deviation grows with the increase of deformation.

2. MATHEMATICAL MODEL AND NUMERICAL IMPLEMENTATION

2.1. Mathematical Model. The study used two fluid reservoirs of height H and width $2W$ connecting a membrane implanted with an individual nanopore of half-width b and length h, as schematically shown in Figure 1. The nanopore and two reservoirs are saturated
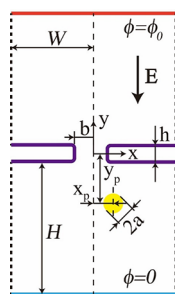

Figure 1. Schematic diagram of transport of the nanoparticle through a nanopore.

with KCl solution with dynamic viscosity μ, density ρ_f, permittivity ε, and bulk salt concentration c_0. The initial position of a circular nanoparticle with radius a and shear modulus G_0 is located at (x_p, y_p). A potential difference ϕ_0 is imposed between the ends of reservoirs, which generates an ionic current through the nanopore. For a negatively charged nanoparticle, it translocates from the cathode reservoir through the nanopore toward the anode reservoir because of electrophoresis. Due to the depletion of the fluid inside the nanopore by the particle's volume, the ionic current when the nanoparticle is inside the nanopore is different from that when it is outside of the nanopore, which generates the current deviation signal. The current deviation signal depends on many factors such as the bulk salt concentration, particle's properties such as size, shape, and the surface charge density. Because the particle's deformation alters the particle's size and shape, it is expected that the particle's deformation will also affect the current deviation signal.

Here we use Poisson−Nernst−Planck equations to describe the ionic mass transport of each ion:

$$-\varepsilon \nabla^2 \phi = F(z_1 c_1 + z_2 c_2) \tag{1}$$

$$\frac{\partial c_i}{\partial t} + \nabla \cdot \mathbf{N}_i = 0, \quad i = 1 \text{ and } 2 \tag{2}$$

ϕ represents the electric potential of the fluid; F is the Faraday constant; z_1 and z_2 are the valences of cations ($z_1 = 1$ for K$^+$) and anions ($z_2 = -1$ for Cl$^-$), respectively; c_1 and c_2 are the molar

concentrations for the cations (K$^+$) and anions (Cl$^-$), respectively; and $\mathbf{N}_i$ is the ionic flux density of the ith ionic species:

$$\mathbf{N}_i = \mathbf{u} c_i - D_i \nabla c_i - z_i \frac{D_i}{RT} F c_i \nabla \phi, \quad i = 1 \text{ and } 2 \tag{3}$$

Here, $\mathbf{u}$ and T respectively represent the velocity and the absolute temperature of the fluid, D_i is the diffusion coefficient of the ith ion, and R is the universal gas constant. Bold letters denote tensors or vectors.

The flow field is simplified by the Stokes equations without considering the inertial terms for low Reynolds number:

$$\rho_f \frac{\partial \mathbf{u}}{\partial t} = \nabla \cdot [-p\mathbf{I} + \mu(\nabla \mathbf{u} + \nabla \mathbf{u}^T)] + \mathbf{f} \tag{4}$$

and

$$\nabla \cdot \mathbf{u} = 0 \tag{5}$$

where p is the pressure of the fluid, and the electrostatic body force, $\mathbf{f} = -F(z_1 c_1 + z_2 c_2) \nabla \phi$.

For incompressible Neo-Hookean material of the particle, and its deformation and motion is governed by

$$\rho_p \frac{\partial^2 \mathbf{S}_p}{\partial t^2} - \nabla \cdot \boldsymbol{\sigma}_p(\mathbf{S}_p) = 0 \tag{6}$$

Where ρ_p and $\mathbf{S}_p$ are, respectively, the density and displacement of the nanoparticle; and $\boldsymbol{\sigma}_p$ is the Cauchy stress of the particle. The normal stress tensor $\boldsymbol{\sigma}_p$ on the nanoparticle-fluid interface is equal to the sum of the hydrodynamic stress tensor $\boldsymbol{\sigma}_f$ and the Maxwell stress tensor $\boldsymbol{\sigma}_E$, described as following:

$$\boldsymbol{\sigma}_p \cdot \mathbf{n}_p = \boldsymbol{\sigma}_f \cdot \mathbf{n}_f + \boldsymbol{\sigma}_E \cdot \mathbf{n}_f \tag{7}$$

$$\boldsymbol{\sigma}_f = -p\mathbf{I} + \mu(\nabla \mathbf{u} + \nabla \mathbf{u}^T) \tag{8}$$

$$\boldsymbol{\sigma}_E = \varepsilon \mathbf{E}\mathbf{E} - \frac{1}{2}\varepsilon(\mathbf{E} \cdot \mathbf{E})\mathbf{I} \tag{9}$$

Here, the electric field intensity is $\mathbf{E} = -\nabla \phi$; $\mathbf{n}_p$ and $\mathbf{n}_f$ are the unit normal vectors of the particle surface and the fluid, respectively, in the reference coordinate system and the space coordinate system.

We choose the particle's radius a, the bulk concentration c_0, RT/F, $\varepsilon R^2 T^2/\mu a F^2$, $\mu U_0/a$, and $\varepsilon R^2 T^2/\mu F$ as the length scale, the ionic concentration scale, the potential scale, the velocity scale, the pressure scale, and the scale of the ionic species diffusivity, respectively. The dimensionless form of the above equation system 1−6 transfers

$$-\nabla^{*2} \phi^* = \frac{1}{2}(\kappa a)^2 (z_1 c_1^* + z_2 c_2^*) \tag{10}$$

$$\frac{\partial c_i^*}{\partial t^*} + \nabla^* \cdot \mathbf{N}_i^* = 0 \tag{11}$$

$$\mathbf{N}_i^* = \mathbf{u}^* c_i^* - D_i^* \nabla^* c_i^* - D_i^* z_i c_i^* \nabla^* \phi^* \tag{12}$$

$$\text{Re} \frac{\partial \mathbf{u}^*}{\partial t^*} = \nabla^* \cdot [-p^*\mathbf{I} + (\nabla^* \mathbf{u}^* + \nabla^* \mathbf{u}^{*T})] + \mathbf{f}^* \tag{13}$$

$$\nabla^* \cdot \mathbf{u}^* = 0 \tag{14}$$

$$\text{Re} \frac{\rho_p}{\rho_f} \frac{\partial^2 \mathbf{S}_p^*}{\partial t^{*2}} - \nabla^* \cdot \boldsymbol{\sigma}(\mathbf{S}_p^*) = 0 \tag{15}$$

In the above, $\kappa^{-1} = \sqrt{\varepsilon RT / \sum_{i=1}^{2} F^2 z_i^2 c_0}$ is the Debye length, and Re $= \rho_f U_0 a / \mu$ is the Reynolds number. The dimensionless variable is represented with a superscript *.

At the ends of the two reservoirs, the boundary conditions of the potential, ionic concentrations, and flow are described as the following:

$$\phi^*(x^*, -(H^* + h^*/2)) = 0 \tag{16}$$

$$\phi*(x*, (H* + h*/2)) = \phi_0^* \tag{17}$$

$$c_i^*(x*, \pm(H* + h*/2)) = 1, \quad i = 1 \text{ and } 2 \tag{18}$$

$$p* = 0 \tag{19}$$

On the surface of the particle, the boundary conditions are as the following:

$$-\mathbf{n} \cdot \nabla*\phi* = \sigma_p^* \tag{20}$$

$$\mathbf{n} \cdot \mathbf{N}_i^* = \mathbf{n} \cdot (\mathbf{u}*c_i^*) \tag{21}$$

$$\mathbf{u}* = \mathbf{u}_p^* = \frac{\partial \mathbf{S}*}{\partial t*} \tag{22}$$

Here, the $\varepsilon RT/Fa$ is used to nondimensionalize the surface charge density.

Assuming that the nanopore wall has a constant surface charge density of σ_w, nonslip (i.e., $u* = 0$), and zero normal ionic flux (i.e., $\mathbf{n} \cdot \mathbf{N}_i^* = 0$) are imposed on the rigid wall of the nanopore. On the side walls of the reservoirs (i.e., the dotted lines in Figure 1), symmetric boundary conditions are adopted for all fields.

The nondimensional total force $\mathbf{F}_p^*$, which is normalized by $a\mu U_0$, includes the electric force $\mathbf{F}_E^*$ and the hydrodynamic force $\mathbf{F}_f^*$, which are evaluated by integrating the nondimensional Maxwell stress tensor $\boldsymbol{\sigma}_E^*$ and hydrodynamic stress tensor $\boldsymbol{\sigma}_i^*$ on the nanoparticle's surface Γ_p^*

$$\mathbf{F}_p^* = \mathbf{F}_E^* + \mathbf{F}_f^* \tag{23}$$

$$\mathbf{F}_E^* = \int \boldsymbol{\sigma}_E^* \cdot \mathbf{n} d\Gamma_p^* = \int \left[\mathbf{E}*\mathbf{E}* - \frac{1}{2}(\mathbf{E}* \cdot \mathbf{E}*)\mathbf{I} \right] \cdot \mathbf{n} d\Gamma_p^* \tag{24}$$

$$\mathbf{F}_f^* = \int \boldsymbol{\sigma}_f^* \cdot \mathbf{n} d\Gamma_p^* = \int [-p*\mathbf{I} + (\nabla*\mathbf{u}* + \nabla*\mathbf{u}^{*T})] \cdot \mathbf{n} d\Gamma_p^* \tag{25}$$

The ionic current normalized by $FU_0C_0a^2$ is

$$I* = \int (z_1\mathbf{N}_1^* + z_2\mathbf{N}_2^*) \cdot \mathbf{n} dS* \tag{26}$$

Here, $S*$ represents the area of either end of the two reservoirs.

2.2. Numerical Implementation and Code Validation. The coupled system of the electric field, ionic transport, particle motion, and deformation is numerically solved. Hughes proposed the ALE method for the first time.[34] Briefly, the mesh moves with the moving particles. When the quality of the mesh is less than a threshold value, a new mesh is generated. Therefore, the ALE method can capture the motion of particles for a long time.

Those dimensionless governing equations are numerically solved by a commercial finite-element package, COMSOL (version 4.3a, www.comsol.com), operating in a high-performance cluster. The initial concentration of each species in the domain is the dimensionless bulk concentration, and other variables are initially zero. To validate our numerical implementation, we simulate the translocation of a cylindrical particle with $\sigma_p^* = -1.0927$ in the nanopore vertically along the centerline, which has uniform parameters as the 2D case presented in work by Ai and Qian,[14] as shown in Figure 2. The parameters used for the case are following: $E* = \phi*/(2H* + h*) = 7.7 \times 10^{-4}$ $(E = 20$ kV/m), $\sigma_w^* = 0$, $G_0 = 1$ GPa, $\kappa a = 1.03$, and 0.46. As the particle is trapped when $\kappa a = 0.46$, only the current deviation for $\kappa a = 1.03$ is shown in Figure 2b. In Figure 2, our numerical results are in good agreement with the numerical results of the particle's velocity and current deviation obtained by Ai and Qian,[14] which have been validated by the analytical solution. The agreement shows that our model is suitable for the study of the nanoparticle moving in the nanopore.
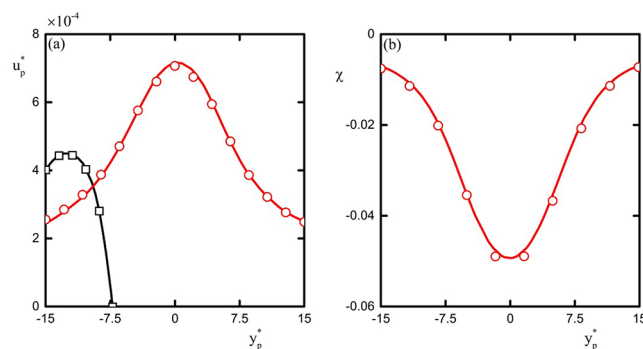
Figure 2. Variations of the (a) y-component translational velocity $u*$ and (b) current deviation χ of the cylinder particle with the particle's location y_p^* under $E* = 7.7 \times 10^{-4}(E = 20$ kV/m), the ratio of the particle radius to the Debye length $\kappa a = 1.03$ (red line and circles) and 0.46 (black lines and squares). Symbols and lines represent, respectively, the numerical solution of Ai and Qian[14] and the numerical results from the present model.

3. RESULTS AND DISCUSSION

The geometry parameters of the nanofluidics and nanoparticle are as follow: $a = 2$ nm, $b = 5$ nm, $h = 5$ nm, $W = 25$ nm, and $H = 40$ nm. The physical parameters include permittivity of the fluid $\varepsilon_f = 80$, the fluid density $\rho_f = 1 \times 10^3$ kg/m^3, the fluid viscosity $\mu = 1 \times 10^{-3}$ Pa s, the temperature of KCl electrolyte aqueous solution $T = 300$ K, the nanoparticle's surface charge density $\sigma_p = -0.01$ C/m^2, the initial position of the particle $y_{p0} = -15$ nm, the diffusivity of K^+ is $D_1 = 1.95 \times 10^{-9}$ m^2/s and the diffusivity of Cl^- is $D_2 = 2.03 \times 10^{-9}$ m^2/s.

In this section, we will first show the deformation process of the particle during the translocation process. The effects of the applied electric field, the ratio of radius to Debye length, and the electrical properties of the nanopore surface on the deformation, migration velocity, and current deviation of the particles are then discussed, respectively.

3.1. Particle Deformation Process during Translocation. The motion of the nanoparticle affects the electric field around the particle, ionic concentration, and flow field, which in turn affect the particle's movement and deformation. Figure 3 depicts the trajectory and shape of the particle with the shear modulus $G_0 = 0.05$ MPa (seen in Movie S1 and
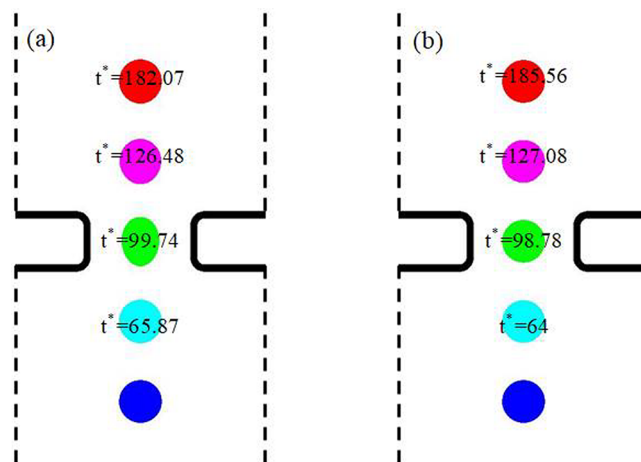
Figure 3. Moving process of the particle under $E* = 0.15$, $x_{p0}^* = 0$, $\kappa a = 1.03$, $\sigma_w = 0$ at (a) $G_0 = 0.05$ MPa and (b) $G_0 = 1$ GPa. The corresponding $y_p^* = -7.5, -3.75, 0, 3.75,$ and 7.5.
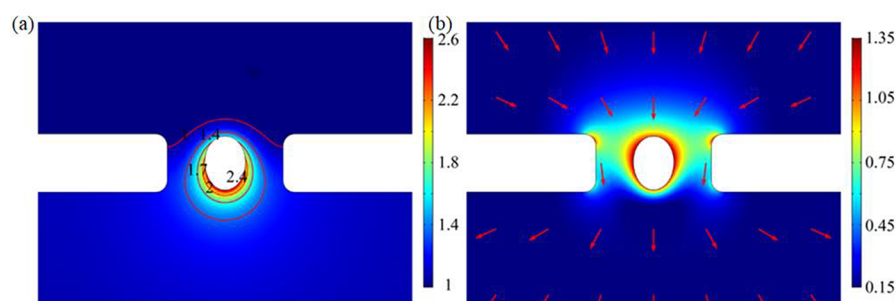
Figure 4. (a) Spatial distribution of c_1^* and (b) norm of electric field intensity around the particle under $E^* = 0.15$. Here $x_{p0}^* = 0, \kappa a = 1.03$, $\sigma_w = 0$, $G_0 = 0.05$ MPa. The color bars and lines denote the dimensionless concentration of cation (K^+) in a and electric field line in b.
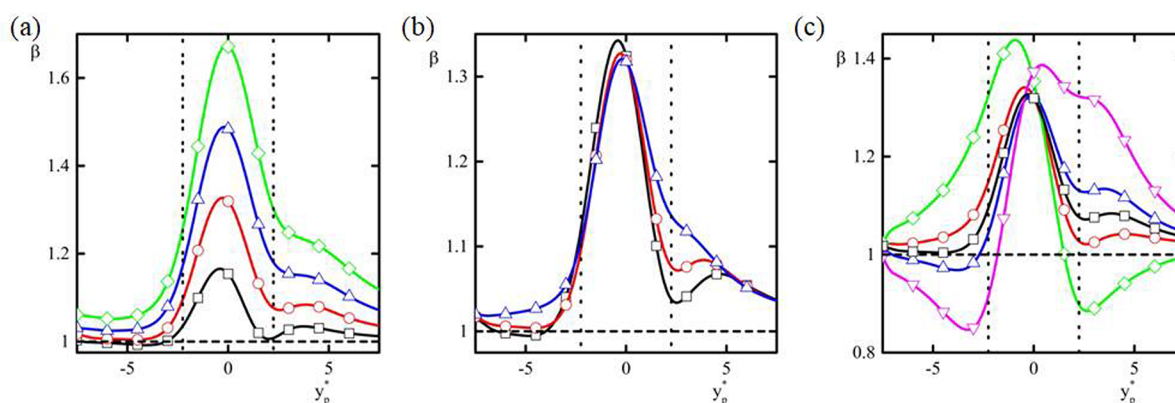

Figure 5. (a) Variations in the ratio β of the major (y-direction) to minor (x-direction) axis of the particle with the particle's location y_p^* under $E^* = 7.7 \times 10^{-2}$ ($E = 1000$ kV/m, black lines and squares), $E^* = 0.15$ ($E = 2000$ kV/m, red lines and circles), $E^* = 0.23$ ($E = 3000$ kV/m, blue lines and triangles), $E^* = 0.31$ ($E = 4000$ kV/m, green lines and rhombuses), here $x_{p0}^* = 0$, $\kappa a = 1.03$, $\sigma_w = 0$, $G_0 = 0.05$ MPa. The dashed line is the result for the particle with $G_0 = 1$ GPa. (b) Variations in the ratio β of the major (y-direction) to the minor (x-direction) axis of the particle with the particle's location y_p^* under $\kappa a = 0.65$ (black lines and squares), $\kappa a = 1.03$ (red lines and circles), $\kappa a = 2.05$ (blue lines and triangles), here $x_{p0}^* = 0$, $\sigma_w = 0$, $E^* = 0.15$, $G_0 = 0.05$ MPa. The dashed line is the result for the particle with $G_0 = 1$ GPa. (c) Variations in the ratio β of the major (y-direction) to minor (x-direction) axis of the particle with y_p^* under $\sigma_w = 0$ (black lines and squares), $\sigma_w^* = -0.1\sigma_p^*$ (red lines and circles), $\sigma_w^* = 0.1\sigma_p^*$ (blue lines and triangles), $\sigma_w^* = -0.4\sigma_p^*$ (green lines and circles), $\sigma_w^* = 0.4\sigma_p^*$ (magenta lines and anti triangles), here $x_{p0}^* = 0$, $\kappa a = 1.03$, $E^* = 0.15$, $G_0 = 0.05$ MPa. The dashed line is the result of the particle with $G_0 = 1$ GPa.

Figure S1) and $G_0 = 1$ GPa (seen in Movie S2 and Figure S1) when $x_{p0} = 0$ and the imposed axial electric field $E^* = 0.15(E = 2000$ kV/m).When the particle with the shear modulus $G_0 = 0.05$ MPa and $G_0 = 1$ GPa are located in Figure 3, the corresponding dimensionless time for Figure 3a, b is, respectively, 65.87 and 64.00, 99.74 and 98.78, 126.48 and 127.08, 182.07, and 185.56. Because the particle is initially located along the centerline of the nanopore, the particle only translocates along the centerline without any lateral displacement in the cathode reservoir prior to entering the nanopore, and the particle keeps a circle and has no significant deformation. Within the nanopore, the nanoparticle with relatively low shear modulus tends to deform gradually into an elliptical shape, as shown in Figure 3a. This deformation is very similar to the particle deformation in the Morshed's research.[27] After the particle exits the nanopore, the deformable particle returns to the original circular shape. For a particle with relatively large shear modulus (Figure 3b), the particle shape remains unchanged during the translocation process. The initial positions of the particles in Figure 3a, b are the same. On the basis of the time shown in Figure 3, the particle with $G_0 = 0.05$ MPa arrives at the nanopore's center at $t^* = 99.74$, whereas it takes $t^* = 98.78$ for the particle with $G_0 = 1$ GPa to

arrive at the center of the nanopore. This suggests that the deformable particle enters the nanopore slower than the rigid particle under other uniform conditions. In addition, the deformable particle takes less time to exit the nanopore, and the whole translocation process for the deformable particle is shorter than that of the rigid one. It must be noted that in numerical simulation, particles above $G_0 = 1$ GPa hardly deform, so in this study, particles with shear modulus with $G_0 = 1$ GPa can be regard as rigid particles.

To explain the deformation mechanism for the particle with relatively low G_0, the concentration distribution of cation (K^+) around the particle, c_1^*, and the electric field intensity when $x_{p0}^* = 0$, $y_p^* = 0$, and $G_0 = 0.05$ MPa are shown in Figure 4a and b, respectively. Because of the EDL of the particle and its negative surface charge, the particle attracts more K^+ ions to accumulate around its surface. By those interactions between the imposed electric field and K^+ ions, some K^+ ions around the particle move to the lower part of the particle, resulting in the concentration of K^+ ions around the lower part of surface is much larger than that around the upper part (Figure 4a). The asymmetric distribution of the counterions around the particle, which is called concentration polarization phenomenon, exists for both deformable and rigid particles.
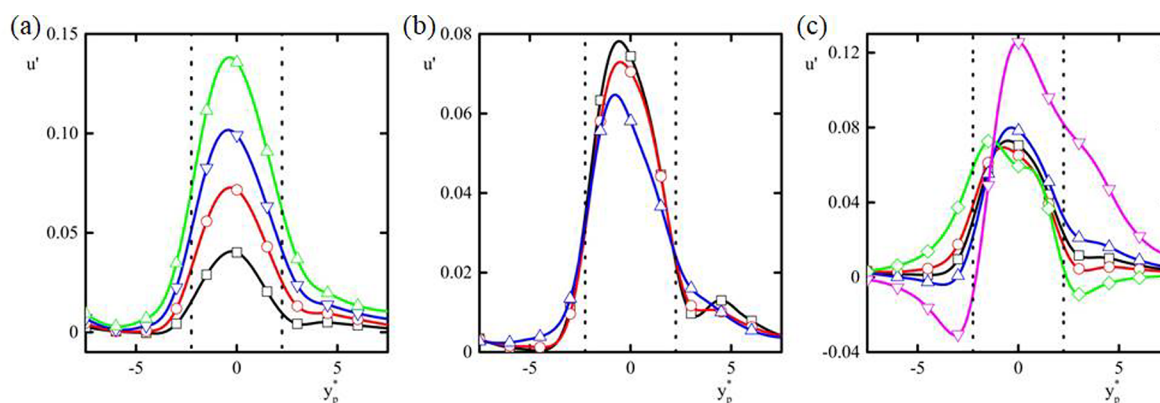
Figure 6. (a) Variations in the translational velocity deviation u' of the particle with the particle's location y_p^* under $E^* = 7.7 \times 10^{-2}$ (black lines and squares), $E^* = 0.15$ (red lines and circles), $E^* = 0.23$ (blue lines and triangles), $E^* = 0.31$ (green lines and rhombuses), here $x_{p0}^* = 0$, $\kappa a = 1.03$, $\sigma_w = 0$. (b) Variations in the y-component translational velocity deviation u' of the particle with the particle's location y_p^* under $\kappa a = 0.65$ (black lines and squares), $\kappa a = 1.03$ (red lines and circles), $\kappa a = 2.05$ (blue lines and triangles); here, $x_{p0}^* = 0$, $\sigma_w = 0$, $E^* = 0.15$. (c) Variations in the y-component translational velocity deviation u' of the particle with the particle's location y_p^* under $\sigma_w = 0$ (black lines and squares), $\sigma_w^* = -0.1\sigma_p^*$ (red lines and circles), $\sigma_w^* = 0.1\sigma_p^*$ (blue lines and triangles), $\sigma_w^* = -0.4\sigma_p^*$ (green lines and rhombuses), $\sigma_w^* = 0.4\sigma_p^*$ (magenta lines and anti triangles); here, $x_{p0} = 0$, $\kappa a = 1.03$, $E^* = 0.15$.

The unbalanced concentration of counterions around the particle generates an electric field on the contrary to the applied one, which develops asymmetric distribution of the electric field surrounding the particle, as shown in Figure 4b.

3.1.1. Influence of the Imposed Electric Field. Figure 3 shows that the particle becomes an elliptical shape when the shear module is relatively low. We define a parameter β, which is the ratio of the major (y-direction) axis to the minor (x-direction) of the elliptical particle, to quantify the deformation of the nanoparticle. Figure 5a depicts β as a function of the location of the nanoparticle under varying imposed electric field intensity E^* when $x_{p0} = 0$ and $G_0 = 0.05$ MPa. The force in the x-direction on the particles is axisymmetric to the y-axis ($x = 0$), leading to the deformation, which is symmetrical to the y-axis ($x = 0$). The particle with relatively high $G_0 = 1$ GPa does not deform and $\beta = 1$ for all electric fields, as shown by the dashed line in Figure 5a as a comparison with the results for $G_0 = 0.05$ MPa. Thus, the case of $G_0 = 1$ GPa corresponds to the case of a rigid particle. The two dotted lines, $y_p^* = \pm 2.25$, correspond to the edges of the nanosilt.

For the particle with $G_0 = 0.05$ MPa, the particle has negligible deform when $y_p^* \leq -7.5$ ($y_p \leq -15$ nm). When the particles move further along the centerline to the nanopore direction, the deformation degree increases and reaches the maximum value when the particles reach the nanopore center, $y_p^* = 0$. As the particle retreats from the pore, the general trend is that β decreases when the particle exits through the pore and enters that anode reservoir. However, at the electric field ($E = 1000$ kV/m and 2000 kV/m), β reaches a local minimum near the edge of the nanopore and then increases as the particles enter the anode reservoir. At a certain distance between the particles and the edge of the nanopore, the local maximum value is reached. When the particles are away from the edge of the pore, they decrease monotonously. The locations for the local minimum and maximum depend on the intensity of the applied electric field. When the electric field intensity is comparatively high, the local minimum and maximum do not appear, as shown by the cases of $E = 3000$ and 4000 kV/m. Furthermore, the profile of β is not symmetric with respect to

$y_p = 0$, and in general, the magnitude of β for positive y_p is larger than that for negative y_p.

Obviously, with the increasing imposed electric field, the deformation of the particle is more significantly with higher value of β. The maximum value of β occurring at $y_p = 0$ for $E = 1000, 2000, 3000,$ and 4000 kV/m are 1.17, 1.33, 1.49, and 1.67, respectively.

3.1.2. Influence of the κa. The nanoparticle deformation is influenced by the value of κa, which increases as the bulk concentration of the electrolyte increases, and affects the ionic concentrations and electric field around the particle.[15,17,19] Figure 5b depicts β as a function of the location of the nanoparticle under different κa. As the particle is away from the pore (i.e., $|y_{p*}| \geq 10$), κa has little influence on the particle deformation. For the case of $\kappa a = 0.65$ (the bulk cation concentration is 10 mol/m³), as the particle approaches the nanopore, it is first compressed with $\beta < 1$, and stretched with $\beta > 1$ as it gets closer to the nanopore. The deformation degree further increases and reaches the maximum prior to the center of the nanopore. After that, its deformation decreases and reaches the local minimum as the particle retreats from the pore. As the particle is outside the pore, the deformation degree further increases, attains a local maximum, and then decreases again when it is further from the nanopore. The result for $\kappa a = 1.03$ (the bulk cation concentration is 25 mol/m³) is very similar to that of $\kappa a = 0.65$ except that β is always greater than 1 during the translocation process. For $\kappa a = 2.05$ (the bulk cation concentration is 100 mol/m³), the local minimum and maximum of β do not exist anymore when the particle exits the nanopore, and the deformation degree monotonically decreases as the particle exits the nanopore. Although κa has an insignificant effect on the maximum value of β, the position of the maximum is more close to the nanopore center as κa increases. In addition, κa has a more significant effect on the particle's deformation as it secedes the pore. During this exiting process, there will be more deformation for the particle as κa increases.

3.1.3. Influence of the Nanopore's Surface Charge Density. Figure 5c depicts β as a function of the position of the nanoparticle when the surface charge densities of nanopore

wall are, respectively, $\sigma_w^* = 0$, $\sigma_w^* = \pm 0.1\sigma_p^*$, and $\sigma_w^* = \pm 0.4\sigma_p^*$. When the nanopore carries opposite charge of the nanoparticle, attractive electrostatic force occurs between the nanopore and the front part of the particle when it approaches the nanopore, and the particle is stretched resulting in $\beta > 1$. When both the nanopore and nanoparticle carry the charges of the same polarity, repulsive electrostatic force between them generates. The repulsive force compresses the particle, leading to $\beta < 1$ before entering the nanopore.

The deformation increases with the increase in the surface charge when $y_p^* < 0$, but it decreases when $y_p^* > 0$. When the wall is positively charged ($\sigma_w^* = -0.1\sigma_p^*$ or $\sigma_w^* = -0.4\sigma_p^*$), the nanopore attracts the particles close to it, which results in the particle being stretched in the y-direction before entering the nanopore. When the particles enter the nanopore, the deformation of the particle decreases rapidly because of the attraction of the nanopore on the particle. On the contrary, when negatively charged ($\sigma_w^* = 0.1\sigma_p^*$ or $\sigma_w^* = 0.4\sigma_p^*$), the nanopore repulsed the particles, which led to the compression of particles in the y-direction before the particles entered the nanopore. It is the notable phenomenon that the deformation β is less than zero. This phenomenon results from electrostatic interaction, which attracts particles when the $y_p^* > 0$ and retards particles when $y_p^* < 0$.

3.2. Translocation Velocity of Deformable Particle.

3.2.1. Influence of the Imposed Electric Field. Under different voltage, the particle's translation velocity varies obviously. To investigate the influence of the applied voltage on the velocity (seen in Figure S2), u' is used to describe the velocity deviation of particles with $G_0 = 0.05$ MPa and $G_0 = 1$ GPa, which is defined as $u' = (u_2 - u_1)/u_{1max}$. Here, u_1 and u_2 are the translation velocity component in the y-direction of particles with $G_0 = 0.05$ MPa and $G_0 = 1$ GPa, respectively, shown in Figure 6a. u_{1max} presents the maximum value of the translation velocity in the y-direction of particles with $G_0 = 1$ GPa. In this section, the applied electric intensity is also $E^* = 7.7 \times 10^{-2}$, 0.15, 0.23, and 0.31. The start (x_p^*, y_p^*) is $(0, -7.5)$. Thus, the particle still migrates along the centerline without lateral displacement. The velocity deviation also increases at first until the velocity reaches its peak point at $y_p^* = 0$ and decreases later. Similar to the particle deformation, the deviation can be ignored, before the edge of particle contacts the inlet of nanopore, namely, $y_p^* = -2.25$. At this moment, the velocity deviation u' is only 0.032. The applied electric intensity is $E^* = 7.7 \times 10^{-2}$, 0.15, 0.23, and 0.31, the largest velocity deviation of particle does not increase linearly with the applied voltage. Here, the largest velocity deviations are respectively 0.041, 0.073, 0.104, and 0.138. Therefore, the velocity of particles with $G_0 = 0.05$ MPa passing through the nanopore is faster than that of rigid particles, and the velocity deviation increases with the increase of electric field strength. This phenomenon is due to the deformation of particles, which is more conducive to the particles passing through the nanopore.

3.2.2. Influence of the κa. The velocity deviation of the particle with the particle's location under same electric field for the different κa is shown in Figure 6b. Same as the subsection above, the particle locates at the centerline in the beginning.

The velocity decreases when the ratio κa increases. When the particle is entering the nanopore, the velocity will decrease because of the repelling of the electro-osmotic flow. As the particle is deformed along the centerline, the repelling hydrodynamic force on the deformable particle is smaller compared to the rigid particle in the center of the nanopore.

Thus, the deformable particle's maximum velocity is higher than the rigid particle's, and the velocity deviation also increases and then decreases (Figure 6b). The velocity reaches the peak point when the center of the particle moves to the origin of coordinates. When the κa increases, the largest velocity deviation decreases. This phenomenon is contributed to the decrease in zeta potential on the surface of particles with the increase in κa, resulting in the decrease in DEP force on particles, the decrease in the maximum velocity of particles passing through nanopores, and the decrease in velocity deviation accordingly. The above phenomenon has also been acknowledged in a previous study.[23] When the κa is 0.65, 1.03, and 2.05, the corresponding largest velocity deviation is 0.078, 0.073, and 0.065.

3.2.3. Influence of the Nanopore's Surface Electrical Property. The surface charge density of a nanopore will change the flow field because of additional electro-osmotic flow (EOF) induced. The EOF sequentially influences the particle translation velocity (Figure 6c). Besides, the nanoparticle and nanopore channel electrostatic interaction produces another impact on particle movement. When the nanopore channel bears positive surface charge ($\sigma_w^* = -0.1\sigma_p^*$ or $\sigma_w^* = -0.4\sigma_p^*$), the channel will attract the particle because of the electrostatic interaction. Furthermore, the electro-osmotic flow generated is in the same direction of particle movement. Thus, the particle will pass through the nanopore more quickly than the noncharged nanopore. In contrast, the generated electro-osmotic flow and the nanoparticle-channel electrostatic interaction take place when the nanopore channel bears negative surface charge ($\sigma_w^* = 0.1\sigma_p^*$ or $\sigma_w^* = 0.4\sigma_p^*$), which hinders the particle from getting into the nanopore. Thus, it will take more time for the particle translating through the nanopore. Similarly, the variation in translocation velocity for the rigid and deformable particle is also investigated because of the particle's deformation. When the nanopore bears a negative charge, the velocity deviation between the particle with $G_0 = 0.05$ MPa and that with $G_0 = 1$ GPa becomes evident. When $\sigma_w^* = 0.4\sigma_p^*$, especially, the velocity for the particle with $G_0 = 0.05$ MPa is only 96.9% of that with $G_0 = 1$ GPa when the position of the particle is at $y_p^* = -3.122$, but the velocity for the particle with $G_0 = 0.05$ MPa is 12.6% larger than that with $G_0 = 1$ GPa when $y_p^* = -0.015$.

For the particle's lateral displacement to the centerline, the particle will move to the centerline of the nanopore first. The initial lateral displacement of the nanoparticle $x_{p0}^* = 1.25$ is set to study the lateral motion of the particle. The variations in the particle's velocity deviation with the location of the nanoparticle follow the same trend as the particle without lateral displacement, though there are small differences because of the initial lateral shift, which is also consistent with the result of ref 14 (seen in Movies S3−S8 and Figures S3−S5).

3.3. Current Blockade of the Translocating Deformable Particle.

3.3.1. Influence of the Imposed Electric Field. The detectable change in the ionic current due to nanoparticle movement is used for the sensing of the nanoparticle. χ^* is used to describe the current deviation of particles with $G_0 = 0.05$ MPa and $G_0 = 1$ GPa, which is defined as $\chi^* = (\chi_2 - \chi_1)/\chi_{1min}$, $\chi_1 = (I_1 - I_0)/I_0$, $\chi_2 = (I_2 - I_0)/I_0$. Here I_1 and I_2 represent the ionic current of particles with $G_0 = 1$ GPa and $G_0 = 0.05$ MPa, respectively. $\chi_{1\,min}$ represents the minimum value of the ionic current of particles with $G_0 = 1$ GPa. Although I_0 is the base current numerically obtained by eq 26 without the particle considered in the simulation. It is noteworthy that
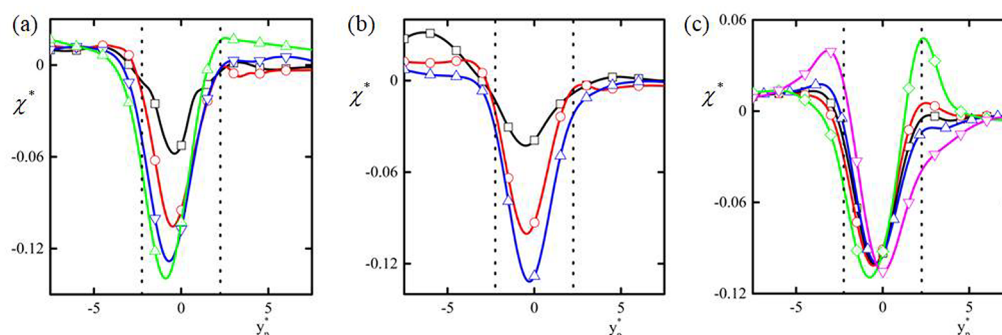
Figure 7. (a) Variations in the current deviation χ^* with the particle's location y_p^* under $E^* = 7.7 \times 10^{-2}$ (black lines and squares), $E^* = 0.15$ (red lines and circles), $E^* = 0.23$ (blue lines and triangles), $E^* = 0.31$ (green lines and rhombuses); here, $x_{p0}^* = 0$, $\kappa a = 1.03$, $\sigma_w = 0$. (b) Variations in the current deviation χ^* with the particle's location y_p^* under $\kappa a = 0.65$ (black lines and squares), $\kappa a = 1.03$ (red lines and circles), $\kappa a = 2.05$ (blue lines and triangles); here, $x_{p0}^* = 0$, $\sigma_w = 0$, $E^* = 0.15$. (c) Variations in the current deviation χ^* with the particle's location y_p^* under $\sigma_w = 0$ (black lines and squares), $\sigma_w^* = -0.1\sigma_p^*$ (red lines and circles), $\sigma_w^* = 0.1\sigma_p^*$ (blue lines and triangles), $\sigma_w^* = -0.4\sigma_p^*$ (green lines and rhombuses), $\sigma_w^* = 0.4\sigma_p^*$ (magenta lines and anti triangles); here, $x_{p0}^* = 0$, $\kappa a = 1.03$, $E^* = 0.15$. The dotted lines are, respectively, $y_p^* = -2.25$ and $y_p^* = 2.25$.

when the ionic current of particles with $G_0 = 0.05$ MPa passing through the nanopore is larger than that of rigid particles, the ionic current deviation χ^* is less than 0, which means that the ion current of the particles with $G_0 = 0.05$ MPa passing through the nanopore is more than that of the rigid particle passing through the nanopore, and vice versa.

The current deviation χ^* for the moving particle with shear modulus $G_0 = 0.05$ MPa and $G_0 = 1$ GPa as a function of the location of the particle under $E^* = 7.7 \times 10^{-2}$, 0.15, 0.23, and 0.31 is shown in Figure 7a. The movement of deformable and rigid nanoparticles in the nanopore block the ionic flow, which brings about decline of the ionic current compared with I_0. When the same κa is employed, the EDL's thickness around the particle remains unchanged. The deformed particle has less of a choking effect on the ion current, which is approximate with I_0. Thus, the current deviation is χ^* below zero. The current deviation under this electric field intensity is relatively small, as deformation is negligible. For the same reason, the curves are almost overlaying before the particle enters and after the particle exits the nanopore. When $E^* = 0.15$ and the center of the particle y_p^* locates at $y_p^* = -2.25$, the edge of particle contacts the inlet of the nanopore. At this moment, the current deviation χ^* is only 0.011. Even $E^* = 0.31$ and $y_p^* = -2.25$, the current deviation χ^* is only -0.069. The applied electric intensity is $E^* = 7.7 \times 10^{-2}$, 0.15, 0.23, and 0.31, and the largest current deviation of the particle does not increase linearly with the applied voltage. Here, the minimum current deviation is -0.058, -0.105, -0.128, and -0.140, respectively. Thus, the particle deformation needs to be considered for the nanopore particle sensing because of the change in the ionic current.

3.3.2. Influence of the κa. In general, the current deviation will be influenced by the EDL thickness and particle deformability. Mostly, a thicker EDL will attract more ions into nanopore. Similar to Figure 7b, the current deviation χ^* can be ignored before the end of particle contacts the inlet of nanopore. The current deviation χ^* reaches the peak point when the center of the particle moves to the origin of coordinates. When the ratio κa is 0.65, 1.03, and 2.05, the minimum current deviation is -0.044, -0.105, and -0.132. The effect of the κa on current is more intense than the effect of the κa on deformation and velocity. The phenomenon is

related to the peak of the amount of the cations. The number of cations would reach the largest value due to the interaction between the channel wall and the double layer around the particle, the thickness of EDL will increase as κa decrease. The current blockade related to cations number can influence the peak point of current deviation. Therefore, compared with the rigid particle, the ion current of the particles with $G_0 = 0.05$ MPa is larger, and the minimum ion current deviation decreases with the increase in the κa.

3.3.3. Influence of the Nanopore's Surface Electrical Property. The nanopore's surface charge density has an obvious influence upon the current value when the particle translates through the pore; the difference of ion current deviation is mainly focused on the period when particles enter the nanopore and exit the nanopore, as shown in Figure 7c. When the nanopore is negatively charged ($\sigma_w^* = 0.1\sigma_p^*$ or $\sigma_w^* = 0.4\sigma_p^*$), the β of deformable particles entering the nanopore is less than 1, and the particles are flattened, which enhances the block of particles to ions, so the ion current caused by the deformable particles passing through the nanopore is smaller than that caused by the rigid particles. Similarly, under positively charged condition of the nanopore ($\sigma_w^* = -0.1\sigma_p^*$ or $\sigma_w^* = -0.4\sigma_p^*$), the β of particles exiting the nanopore is less than 1, which makes the ion current caused by the deformable particles passing through the nanopore is smaller than that caused by the rigid one. When the nanopore bears a positive charge ($\sigma_w^* = -0.4\sigma_p^*$), the current deviation arrives at the summit and the maximum is 0.048. Nevertheless, when the nanopore's surface bears a negative charge ($\sigma_w^* = 0.4\sigma_p^*$), the summit appears, and it is 0.040.

4. CONCLUSIONS

Herein, we construct an instantaneous continuum-based model for the research of the deformable particle moving through a nanopore for the first time, which solves the coupled system of the Poisson equation for the electric field, the Nernst−Planck equations for the ionic concentrations and the Navier−Stokes equations for the fluid field by the ALE method. The effects of the EDL, the nanopore's surface charge density for the nanoparticle deformation are included in our model. By this developed model, the translation velocity and current deviation of the deformable particle passing through the nanopore are

investigated. To validate our code for particle movement, the rigid particle movement obtained by the presented method is qualitatively consistent with the preceding numerical result.

The nanoparticle deforming process shows that the circular particle changes to ellipse when entering the pore then arrives at the largest deformation in the pore and releases to circular shape when leaving the pore. With the increase in the deformation rate of particles, the transport velocity and ion current of the particle also increase. The increasing of applied electric intensity enhances the force acting on the nanopore surface and thus induces larger deformation. The ratio of the nanoparticle radius to the Debye length κa influences the motion and current deviation of the particle by affecting the ionic concentration around the particle. When the κa is relatively larger, the velocity deviation will be reduced; when the κa is relatively small, the current deviation will be difficult to detect. The different surface charge density of nanopore boundary changes the interaction force of the particle and nanopore. By surface treating the nanopore, the particle transport speed can be reduced without changing the ion current passing through the nanopore. Because of the deformation of the particle, the difference of the movement velocity and ionic current for the rigid and deformable particles can be observed, which needs to be considered when we employ the current deviation for detection signal.

■ ASSOCIATED CONTENT

ⓈⒾ Supporting Information

The Supporting Information is available free of charge at https://pubs.acs.org/doi/10.1021/acsabm.0c00606.

> Simulation conditions of the movies files (Table S1); flow field around the particle under $E^* = 0.15$, $x_{p0}^* = 0$, $\sigma_w^* = 0$, $ka = 1.03$ with different G_0 (Figure S1); variations in the y-component translational velocity u^* of the particle with the particle's location y_p^* under different E^* (Figure S2); flow field around the particle under $E^* = 0.15$, $x_{p0}^* = 1.25$, $\sigma_w^* = 0$, $ka = 1.03$ with different G_0 (Figure S3); flow field around the particle under $E^* = 0.15$, $x_{p0}^* = 1.25$, $\sigma_w^* = -0.1\sigma_p^*$, $ka = 1.03$ with different G_0 (Figure S4); and flow field around the particle under $E^* = 0.15$, $x_{p0}^* = 1.25$, $\sigma_w^* = 0.1\sigma_p^*$, $ka = 1.03$ with different G_0 (Figure S5) (PDF)

> Movie S1, flow field around the particle under E^* ; here $ka = 1.03$, $G_0 = 0.05$ MPa, $\sigma_w^* = 0$; the color bar is the fluid velocity, the cones denote the direction of flow field, and the particle's initial location is $x_{p0}^* = 0$, $y_{p0}^* = -7.5$ (MP4)

> Movie S2, flow field around the particle under E^* ; here $ka = 1.03$, $G_0 = 1$ GPa, $\sigma_w^* = 0$; the color bar is the fluid velocity, the cones denote the direction of flow field, and the particle's initial location is $x_{p0}^* = 0$, $y_{p0}^* = -7.5$ (MP4)

> Movie S3, flow field around the particle under E^* ; here $ka = 1.03$, $G_0 = 0.05$ MPa, $\sigma_w^* = 0$; the color bar is the fluid velocity, the cones denote the direction of flow field, and the particle's initial location is $x_{p0}^* = 1.25$, $y_{p0}^* = -7.5$ (MP4)

> Movie S4, flow field around the particle under E^* ; here $ka = 1.03$, $G_0 = 1$ GPa, $\sigma_w^* = 0$; the color bar is the fluid velocity, the cones denote the direction of flow field, and the particle's initial location is $x_{p0}^* = 1.25$, $y_{p0}^* = -7.5$ (MP4)

> Movie S5, flow field around the particle under E^* ; here $ka = 1.03$, $G_0 = 0.05$ MPa, $\sigma_w^* = -0.1\sigma_p^*$; the color bar is the fluid velocity, the cones denote the direction of flow field, and the particle's initial location is $x_{p0}^* = 1.25$, $y_{p0}^* = -7.5$ (MP4)

> Movie S6, flow field around the particle under E^* ; here $ka = 1.03$, $G_0 = 1$ GPa, $\sigma_w^* = -0.1\sigma_p^*$; the color bar is the fluid velocity, the cones denote the direction of flow field, and the particle's initial location is $x_{p0}^* = 1.25$, $y_{p0}^* = -7.5$ (MP4)

> Movie S7, flow field around the particle under E^* ; here $ka = 1.03$, $G_0 = 0.05$ MPa, $\sigma_w^* = 0.1\sigma_p^*$; the color bar is the fluid velocity, the cones denote the direction of flow field, and the particle's initial location is $x_{p0}^* = 1.25$, $y_{p0}^* = -7.5$ (MP4)

> Movie S8, flow field around the particle under E^* ; here $ka = 1.03$, $G_0 = 1$ GPa, $\sigma_w^* = 0.1\sigma_p^*$; the color bar is the fluid velocity, the cones denote the direction of flow field, and the particle's initial location is $x_{p0}^* = 1.25$, $y_{p0}^* = -7.5$ (MP4)

■ AUTHOR INFORMATION

Corresponding Author

Teng Zhou − *Mechanical and Electrical Engineering College, Hainan University, Haikou 570228, Hainan, China;* ⓞ orcid.org/0000-0002-8744-9083; Email: zhouteng@hainanu.edu.cn

Authors

Jian Ge − *Mechanical and Electrical Engineering College, Hainan University, Haikou 570228, Hainan, China*

Liuyong Shi − *Mechanical and Electrical Engineering College, Hainan University, Haikou 570228, Hainan, China*

Zhenyu Liu − *State Key Laboratory of Applied Optics, Changchun Institute of Optics, Fine Mechanics and Physics (CIOMP), Chinese Academy of Sciences, Changchun 130033, China*

Yongbo Deng − *State Key Laboratory of Applied Optics, Changchun Institute of Optics, Fine Mechanics and Physics (CIOMP), Chinese Academy of Sciences, Changchun 130033, China*

Yinyin Peng − *Mechanical and Electrical Engineering College, Hainan University, Haikou 570228, Hainan, China*

Xiaohan He − *Mechanical and Electrical Engineering College, Hainan University, Haikou 570228, Hainan, China*

Rongnian Tang − *Mechanical and Electrical Engineering College, Hainan University, Haikou 570228, Hainan, China*

Liping Wen − *CAS Key Laboratory of Bio-inspired Materials and Interfacial Science, Technical Institute of Physics and Chemistry, Chinese Academy of Sciences, Beijing 100190, China;* ⓞ orcid.org/0000-0001-8546-8988

Complete contact information is available at:
https://pubs.acs.org/10.1021/acsabm.0c00606

Notes

The authors declare no competing financial interest.

■ ACKNOWLEDGMENTS

■ REFERENCES

(1) Li, Z. R.; Liu, W.; Gong, L. Y.; Zhu, Y. D.; Gu, Y. T.; Han, J. Accurate Multi-Physics Numerical Analysis of Particle Preconcentration Based on Ion Concentration Polarization. *Int. J. Appl. Mech* **2017**, *9* (8), 1750107.

(2) Xiao, K.; Wen, L.; Jiang, L. Biomimetic Solid-State Nanochannels: From Fundamental Research to Practical Applications. *Small* **2016**, *12* (21), 2810−31.

(3) Ma, J.; Qiu, Y.; Yuan, Z.; Zhang, Y.; Sha, J.; Liu, L.; Sun, L.; Ni, Z.; Yi, H.; Li, D.; Chen, Y. Detection of short single-strand DNA homopolymers with ultrathin Si3N4 nanopores. *Phys. Rev. E* **2015**, *92* (2), No. 022719.

(4) Zhang, M. K.; Yeh, L. H.; Qian, S. Z.; Hsu, J. P.; Joo, S. W. DNA Electrokinetic Translocation through a Nanopore: Local Permittivity Environment Effect. *J. Phys. Chem. C* **2012**, *116* (7), 4793−4801.

(5) Habibi Matin, M.; Salimi, S.; Yaghoobi, A. Influence of Biofluids Rheological Behavior on Electroosmotic Flow and Ionic Current Rectification in Conical Nanopores. *J. Phys. Chem. C* **2016**, *120* (50), 28832−28843.

(6) Hsu, J. P.; Chen, Y. M.; Yang, S. T.; Lin, C. Y.; Tseng, S. Influence of salt valence on the rectification behavior of nanochannels. *J. Colloid Interface Sci.* **2018**, *531*, 483−492.

(7) Zhang, Y.; Wu, G.; Si, W.; Ma, J.; Yuan, Z.; Xie, X.; Liu, L.; Sha, J.; Li, D.; Chen, Y. Ionic current modulation from DNA translocation through nanopores under high ionic strength and concentration gradients. *Nanoscale* **2017**, *9* (2), 930−939.

(8) Li, J.; Gershow, M.; Stein, D.; Brandin, E.; Golovchenko, J. A. DNA molecules and configurations in a solid-state nanopore microscope. *Nat. Mater.* **2003**, *2* (9), 611−5.

(9) An, N.; Fleming, A. M.; White, H. S.; Burrows, C. J. Nanopore detection of 8-oxoguanine in the human telomere repeat sequence. *ACS Nano* **2015**, *9* (4), 4296−307.

(10) Venkatesan, B. M.; Bashir, R. Nanopore sensors for nucleic acid analysis. *Nat. Nanotechnol.* **2011**, *6* (10), 615−24.

(11) Lin, C. Y.; Hsu, J. P.; Yeh, L. H. Rectification of ionic current in nanopores functionalized with bipolar polyelectrolyte brushes. *Sens. Actuators, B* **2018**, *258*, 1223−1229.

(12) Campos, E. J.; Yates, J. Single molecule characterisation of metal nanoparticles using nanopore-based stochastic detection methods. *Sens. Actuators, B* **2018**, *255*, 2032−2049.

(13) Deamer, D.; Akeson, M.; Branton, D. Three decades of nanopore sequencing. *Nat. Biotechnol.* **2016**, *34* (5), 518−24.

(14) Ai, Y.; Qian, S. Electrokinetic particle translocation through a nanopore. *Phys. Chem. Chem. Phys.* **2011**, *13* (9), 4060−71.

(15) Ai, Y.; Liu, J.; Zhang, B.; Qian, S. Field effect regulation of DNA translocation through a nanopore. *Anal. Chem.* **2010**, *82* (19), 8217−25.

(16) Zhang, M.; Ai, Y.; Sharma, A.; Joo, S. W.; Kim, D. S.; Qian, S. Electrokinetic particle translocation through a nanopore containing a floating electrode. *Electrophoresis* **2011**, *32* (14), 1864−74.

(17) Zhang, M.; Ai, Y.; Kim, D. S.; Jeong, J. H.; Joo, S. W.; Qian, S. Electrophoretic motion of a soft spherical particle in a nanopore. *Colloids Surf., B* **2011**, *88* (1), 165−74.

(18) Yeh, L. H.; Tai, Y. H.; Wang, N.; Hsu, J. P.; Qian, S. Electrokinetics of pH-regulated zwitterionic polyelectrolyte nanoparticles. *Nanoscale* **2012**, *4* (23), 7575−84.

(19) Zhou, C.; Mei, L. J.; Su, Y. S.; Yeh, L. H.; Zhang, X. Y.; Qian, S. Z. Gated ion transport in a soft nanochannel with biomimetic polyelectrolyte brush layers. *Sens. Actuators, B* **2016**, *229*, 305−314.

(20) Lautner, G.; Plesz, M.; Jagerszki, G.; Furjes, P.; Gyurcsanyi, R. E. Nanoparticle displacement assay with electrochemical nanopore-based sensors. *Electrochem. Commun.* **2016**, *71*, 13−17.

(21) Plesa, C.; van Loo, N.; Ketterer, P.; Dietz, H.; Dekker, C. Velocity of DNA during Translocation through a Solid-State Nanopore. *Nano Lett.* **2015**, *15*, 732−737.

(22) Aksimentiev, A. Deciphering ionic current signatures of DNA transport through a nanopore. *Nanoscale* **2010**, *2* (4), 468−83.

(23) Liu, H.; Qian, S.; Bau, H. H. The effect of translocating cylindrical particles on the ionic current through a nanopore. *Biophys. J.* **2007**, *92* (4), 1164−77.

(24) Luan, B.; Stolovitzky, G.; Martyna, G. Slowing and controlling the translocation of DNA in a solid-state nanopore. *Nanoscale* **2012**, *4* (4), 1068−77.

(25) Branton, D.; Deamer, D. W.; Marziali, A.; Bayley, H.; Benner, S. A.; Butler, T.; Di Ventra, M.; Garaj, S.; Hibbs, A.; Huang, X.; Jovanovich, S. B.; Krstic, P. S.; Lindsay, S.; Ling, X. S.; Mastrangelo, C. H.; Meller, A.; Oliver, J. S.; Pershin, Y. V.; Ramsey, J. M.; Riehn, R.; Soni, G. V.; Tabard-Cossa, V.; Wanunu, M.; Wiggin, M.; Schloss, J. A. The potential and challenges of nanopore sequencing. *Nat. Biotechnol.* **2008**, *26* (10), 1146−53.

(26) Meller, A.; Nivon, L.; Branton, D. Voltage-driven DNA translocations through a nanopore. *Phys. Rev. Lett.* **2001**, *86* (15), 3435−8.

(27) Morshed, A.; Dutta, P.; Kim, M. J. Electrophoretic transport and dynamic deformation of bio-vesicles. *Electrophoresis* **2019**, *40* (18−19), 2584−2591.

(28) Bao, G.; Suresh, S. Cell and molecular mechanics of biological materials. *Nat. Mater.* **2003**, *2* (11), 715−25.

(29) Seeman, N. C. DNA in a material world. *Nature* **2003**, *421* (6921), 427−31.

(30) Yeh, L. H.; Zhang, M.; Qian, S.; Hsu, J. P. Regulating DNA translocation through functionalized soft nanopores. *Nanoscale* **2012**, *4* (8), 2685−93.

(31) Zhou, T.; Ge, J.; Shi, L.; Fan, J.; Liu, Z.; Woo Joo, S. Dielectrophoretic choking phenomenon of a deformable particle in a converging-diverging microchannel. *Electrophoresis* **2018**, *39* (4), 590−596.

(32) Zhou, T.; Liu, Z.; Wu, Y.; Deng, Y.; Liu, Y.; Liu, G. Hydrodynamic particle focusing design using fluid-particle interaction. *Biomicrofluidics* **2013**, *7* (5), 054104.

(33) Zhou, T.; Shi, L. Y.; Fan, C. L.; Liang, D.; Weng, S. J.; Joo, S. W. A novel scalable microfluidic load sensor based on electrokinetic phenomena. *Microfluid. Nanofluid.* **2017**, *21* (4), 59.

(34) Hughes, T. J. R.; Liu, W. K.; Zimmermann, T. K. Lagrangian-Eulerian finite element formulation for incompressible viscous flows. *Comput. Meth. Appl. Mech. Eng.* **1981**, *29* (3), 329−349.